Electronic Supplementary Material (ESI) for Dalton Transactions.

Supporting Information

A Three-Dimensional Mn-Based MOF as a High-Performance Supercapacitor Electrode

Hongren Rong[a], Peng Song[a], Gexiang Gao[a], Qingyan Jiang [a], Xiaojuan Chen[a], Lixin Su [a], Wen-Long Liu[b]*, Qi Liu[a]*

[a]Jiangsu Key Laboratory of Advanced Catalytic Materials and Technology, Advanced Catalysis and Green Manufacturing Collaborative Innovation Center and School of Petrochemical Engineering, Changzhou University, Changzhou, Jiangsu 213164, P. R. China.

[b]School of Chemistry and Chemical Engineering, Yangzhou University, Yangzhou Jiangsu 225009, P. R. China

1. Scheme, Figures and Tables

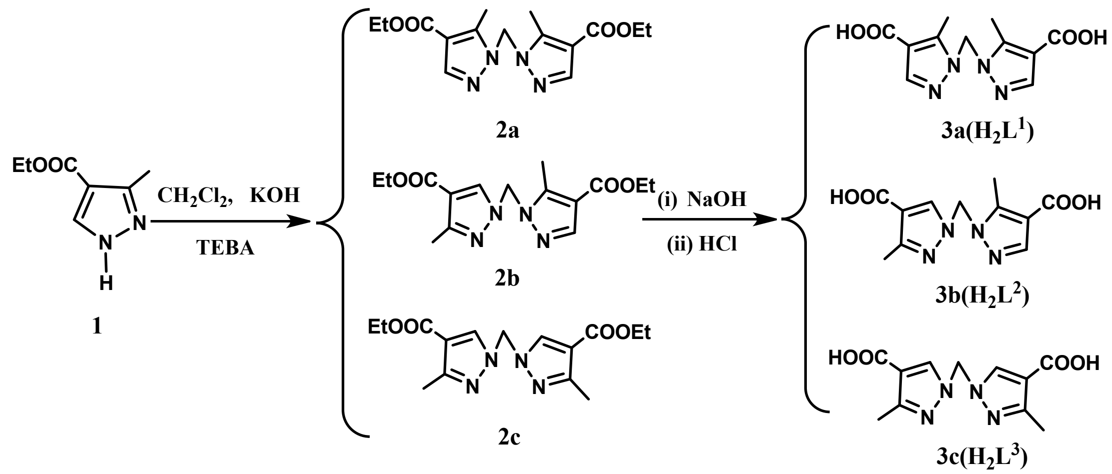

Scheme S1 Synthetic route of the ligands H_2L^1, H_2L^2 and H_2L^3

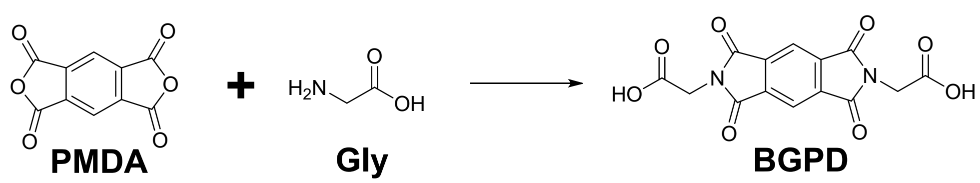

Scheme S2. Synthetic route of BGPD

Table S1 The main bond length (Å) and bond angle (°) of Mn-BGPD

Mn-BGPD			
Mn(1)-O(2)	2.1737(19)	Mn(1)-O(1)C	2.1991(19)
Mn(1)-O(2)A	2.1738(19)	Mn(1)-O(5)A	2.1825(19)
Mn(1)-O(5)	2.1826(19)	Mn(1)-O(1)B	2.1991(19)
O(2)-Mn(1)-O(2)A	180.0	O(2)-Mn(1)-O(1)C	92.05(7)
O(2)-Mn(1)-O(1)B	87.95(7)	O(2)A-Mn(1)-O(1)C	87.95(7)
O(2)A-Mn(1)-O(1)B	92.05(7)	O(5)A-Mn(1)-O(1)B	88.57(8)
O(2)-Mn(1)-O(5)A	89.54(7)	O(5)A-Mn(1)-O(1)C	91.43(8)
O(2)A-Mn(1)-O(5)A	90.46(7)	O(5)-Mn(1)-O(1)C	88.57(8)
O(2)-Mn(1)-O(5)	90.46(7)	O(1)B-Mn(1)-O(1)C	180.0
O(2)A-Mn(1)-O(5)	89.54(7)	O(5)A-Mn(1)-O(5)	180.0
O(5)-Mn(1)-O(1)B	91.43(8)		

Symmetry codes: A -x+1,-y+1,-z+1; B -x+1,y-1/2,-z+3/2; C x,-y+3/2,z-1/2

Table S2 The bond length (Å) and bond angle (°) of the hydrogen bond of Mn-BGPD

D–H···A	D–H	H···A	D···A	∠D–H···A
O(5)-H(5A)...O(1)#1	0.96	1.90	2.7150	141.00
O(5)-H(5B)...O(3)#8	0.96	2.02	2.8230	140.00
C(2)-H(2A)...O(5)#6	0.97	2.62	3.553	161.00
C(2)-H(2B)...O(2)#7	0.97	2.44	3.1349	128.00

Symmetry codes:#1 -x+1,-y+1,-z+1; #2 -x+1,y-1/2,-z+3/2; #3 x,-y+3/2,z-1/2; #4 -x,-y+1,-z+1; #5 -x+1,y+1/2,-z+3/2; #6 x,y,z+1; #7 x,-y+3/2,z+1/2; #8 x,-y+1/2,z-1/2

Table S3 Performance comparison of the reported MOFs-based electrodes

Electrodes	Electrolyte	Voltage (V)	specific capacitance (F g^{-1})	Ref.
Co-MOF	1 M KOH	0-0.47	446.8 F g^{-1} at 1.2 A g^{-1}	[27]
Ni-MOF	2 M KOH	0-0.4	726 F g^{-1} at 1 A g^{-1}	[31]
SC-1	6 M KOH	0-0.55	705 F g^{-1} at 1 A g^{-1}	[36]
MOF-3	2 M KOH	0-0.38	465 F g^{-1} at 1 A g^{-1}	[37]
Co-MOF	1 M KOH	0-0.6	148 F g^{-1} at 2 A g^{-1}	[38]
SNNU-52	2 M KOH	0-0.5	523 F g^{-1} at 1 A g^{-1}	[39]
Cu@BTC-120	3 M KOH	0-0.5	228 F g^{-1} at 1.5 A g^{-1}	[41]
Ni-CP	7 M KOH	0-0.4	802 F g^{-1} at 3 A g^{-1}	[46]
Mn-BGPD	1 M KOH	0-0.57	832.6 F g^{-1} at 1 A g^{-1}	This work

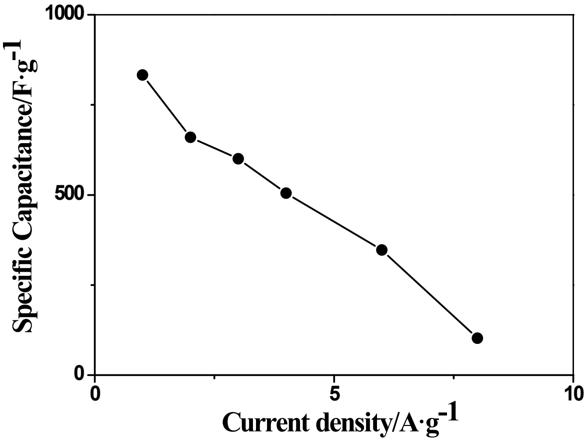

Figure S1 Specific capacitances of the Mn-BGPD electrode at different current densities

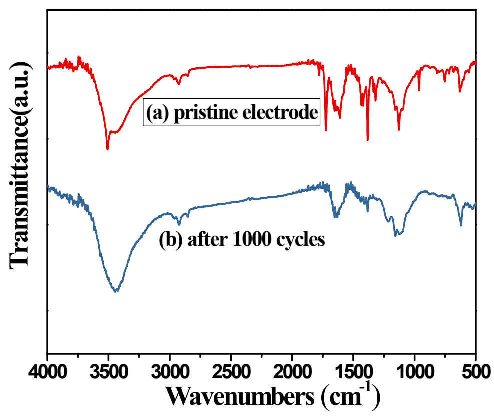

Figure S2. FTIR spectra of the Mn−BGPD (a) pristine electrode containing Mn−BGPD, acetylene black, and PTFE. (b) after 1000 cycles.

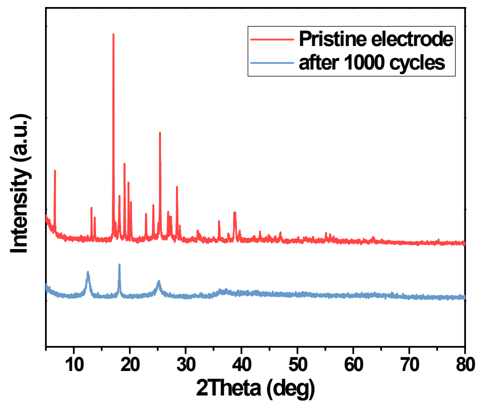

Figure S3. XRD patterns of the Mn−BGPD (a) pristine electrode containing Mn−BGPD, acetylene black, and PTFE. (b) after 1000 cycles.

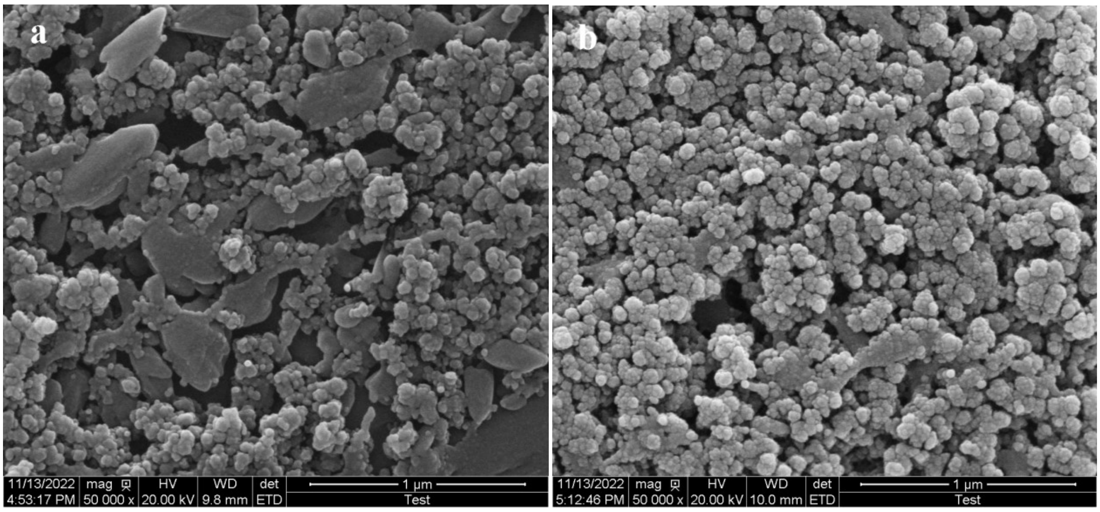

Figure S4. SEM images of the Mn−BGPD (a) pristine electrode containing Mn−BGPD, acetylene black, and PTFE. (b) after 1000 cycles.

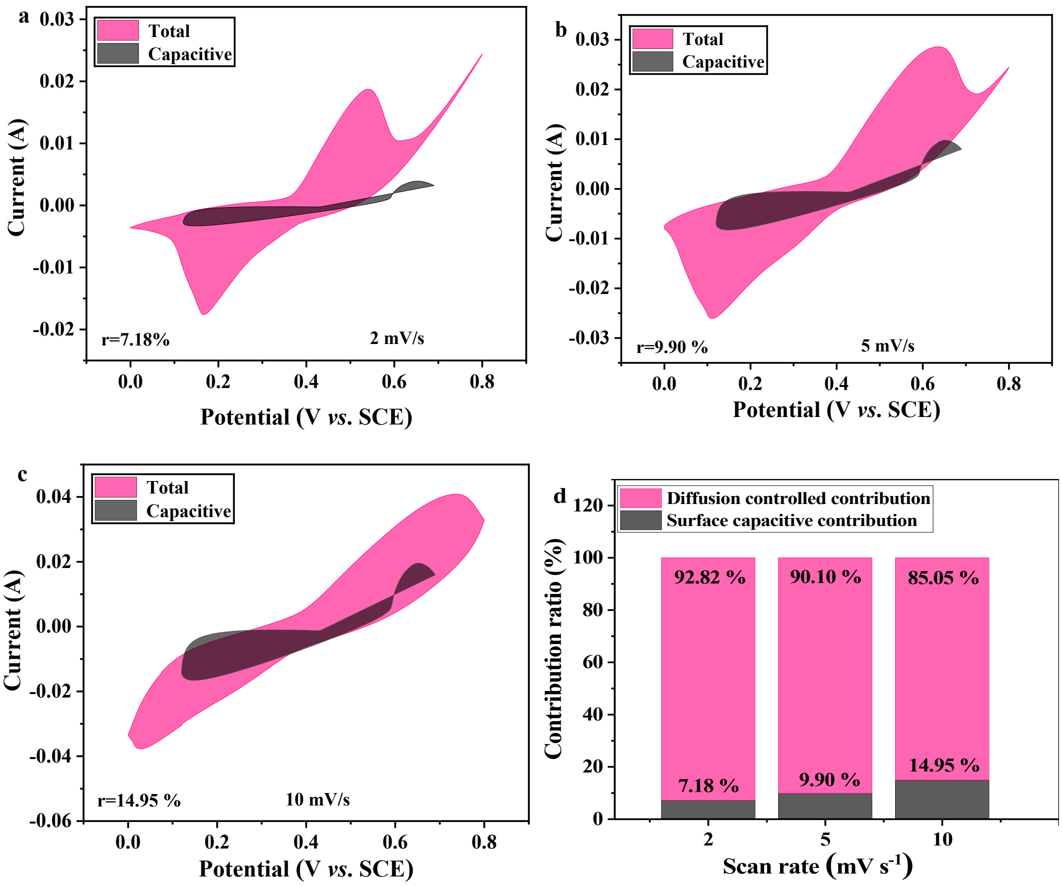

Figure S 5 (a-c) CV curves with capacity separation at different scan rates. (d) The contribution ratios of the diffusion-controlled capacities and capacitive capacities at different scan rates.

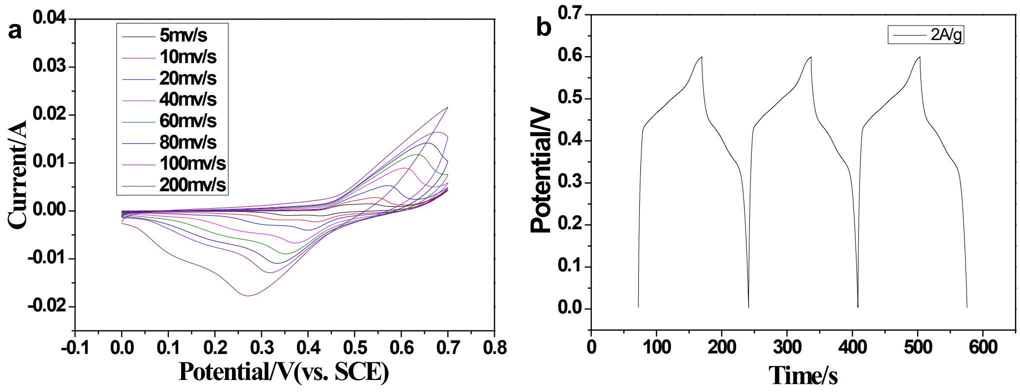

Figure S6. (a) CV curves of the rGO electrode at different scanning rates. (b) The charge-discharge curves of the rGO electrode at the current density of 2A g^{-1}.

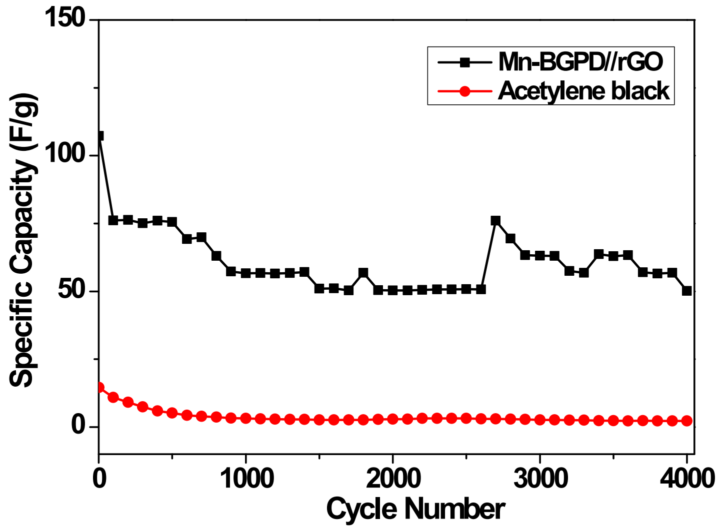

Figure S7. Cyclic performance of the Mn-BGPD//rGO ASC and acetylene black

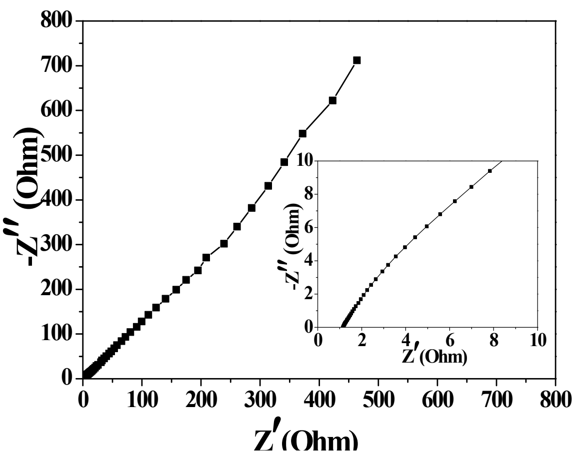

Figure S8. Nyquist plot of the Mn-BGPD//rGO ASC